Clim Dyn (2016) 46:2847–2861
DOI 10.1007/s00382-015-2735-6

How predictable is the anomaly pattern of the Indian summer rainfall?

Juan Li[1,2] · **Bin Wang**[1,2]

Received: 17 November 2014 / Accepted: 29 June 2015 / Published online: 17 July 2015

Abstract Century-long efforts have been devoted to seasonal forecast of Indian summer monsoon rainfall (ISMR). Most studies of seasonal forecast so far have focused on predicting the total amount of summer rainfall averaged over the entire India (i.e., all Indian rainfall index-AIRI). However, it is practically more useful to forecast anomalous seasonal rainfall distribution (anomaly pattern) across India. The unknown science question is to what extent the anomalous rainfall pattern is predictable. This study attempted to address this question. Assessment of the 46-year (1960–2005) hindcast made by the five state-of-the-art ENSEMBLE coupled dynamic models' multi-model ensemble (MME) prediction reveals that the temporal correlation coefficient (TCC) skill for prediction of AIRI is 0.43, while the area averaged TCC skill for prediction of anomalous rainfall pattern is only 0.16. The present study aims to estimate the predictability of ISMR on regional scales by using Predictable Mode Analysis method and to develop a set of physics-based empirical (P–E) models for prediction of ISMR anomaly pattern. We show that the first three observed empirical orthogonal function (EOF) patterns of the ISMR have their distinct dynamical origins rooted in an eastern Pacific-type La Nina, a central Pacific-type La Nina, and a cooling center near dateline, respectively. These equatorial Pacific sea surface temperature anomalies, while located in different longitudes, can all set up a specific teleconnection pattern that affects Indian monsoon and results in different rainfall EOF patterns. Furthermore, the dynamical models' skill for predicting ISMR distribution primarily comes primarily from these three modes. Therefore, these modes can be regarded as potentially predictable modes. If these modes are perfectly predicted, about 51 % of the total observed variability is potentially predictable. Based on understanding the lead–lag relationships between the lower boundary anomalies and the predictable modes, a set of P–E models is established to predict the principal component of each predictable mode, so that the ISMR anomaly pattern can be predicted by using the sum of the predictable modes. Three validation schemes are used to assess the performance of the P–E models' hindcast and independent forecast. The validated TCC skills of the P–E model here are more than doubled that of dynamical models' MME hindcast, suggesting a large room for improvement of the current dynamical prediction. The methodology proposed here can be applied to a wide range of climate prediction and predictability studies. The limitation and future improvement are also discussed.

Keywords Predictability · Predictable mode analysis (PMA) · Indian summer monsoon rainfall · Seasonal prediction · Physics-based empirical prediction model

✉ Bin Wang
wangbin@hawaii.edu

Juan Li
juanl@hawaii.edu

[1] Earth System Modeling Center, Nanjing University of Information Science and Technology, Nanjing 210044, China

[2] Department of Atmospheric Sciences and International Pacific Research Center, University of Hawaii at Manoa, Honolulu, HI 96822, USA

1 Introduction

The Indian summer monsoon rainfall (ISMR) has a crucial impact on Indian agricultural production, water resource and disaster managements. With growing population, India is strongly depending on the rain-fed agriculture (Gadgil

and Gadgil 2006). Due to considerable spatial and temporal variability of ISMR, the seasonal prediction of monsoon rainfall over India became one of the challenging tasks in climate scientific field (Rajeevan 2001; Gadgil et al. 2005; Webster and Hoyos 2010). Making correct seasonal forecast of ISMR distribution is of significance for scientific values and social needs. However, so far very limited studies have focused on prediction of ISMR anomaly pattern.

Tremendous efforts have been made by Indian Meteorological Department (IMD) to predict the total amount of ISMR, i.e., the all Indian rainfall index (AIRI) (Shukla and Mooley 1987; Gowariker et al. 1991; Kumar et al. 1995; Guhathakurta et al. 1999; Rajeevan 2001). Despite advancement in physical understanding and development of advanced statistical models (Rajeevan et al. 2007), the forecast fails in recent years (Rajeevan et al. 2012; Wang et al. 2015b). Dynamical model is an effective and ultimate tool for seasonal forecast, but a number of previous studies found that most of the present dynamic models have limited skills in predicting summer monsoon rainfall over India (Gadgil and Sajani 1998; Kang et al. 2002; Wang et al. 2005; Gadgil and Srinivasan 2011).

In this study, we will show that multi-model ensemble (MME) hindcast made by five state-of-the-arts ENSEMBLE project models (details are introduced in Sect. 2.1) for ISMR pattern prediction has limited skill: the temporal correlation coefficient (TCC) skill averaged over entire India is only 0.16 during the period of 1960–2005. This skill is considerably lower than the TCC skill for MME's prediction of AIRI, which is 0.43, indicating that prediction of the spatial distribution of the ISMR is much more difficult than prediction of the AIRI. An improvement in skill of the downscale prediction of ISMR from a global spectral model is only noticed over some parts of India (Sinha et al. 2013).

Outstanding problems remain: To what extent the ISMR distribution is predictable and what the effective way is for forecasting the ISMR anomaly pattern. The present work attempts to address these critical issues. The key to address these questions is to fully understand the physical processes linking major modes of ISMR and the simultaneous and precursory large-scale lower-boundary anomalies. This is a major effort will be made in this work. It is only with the guidance of this understanding that development of a Physics-based Empirical (P–E) prediction model for ISMR distribution is possible. An additional effort that will be made is to estimate the predictability of ISMR anomaly pattern. A better knowledge of the predictability would facilitate improvement of prediction skills (Lee et al. 2011, 2013).

Section 2 describes the observational data and coupled climate models' hindcast data. The methodology used in the present study are also described in detail, especially the idea of Predictable Mode Analysis, the principles and methodology for selection of physically consequential predictors and for establishment of the P–E models, as well as three ways of validation of the model performance. In Sect. 3, we describe characteristics of the major modes of ISMR variability, explore their origins, and examine the dynamical model's capability in capturing these modes, so that the predictable modes can be identified and the potential predictability of the ISMR distribution can be estimated. Section 4 presents the lead–lag relationship between physical predictors and predictands, and the prediction skills made by the P–E models. Finally, conclusion and discussion are presented in Sect. 5.

2 Data and methodology

2.1 Data

IMD established a large network of rain gauge stations and developed high resolution (1° × 1°) gridded rainfall dataset (Rajeevan et al. 2006, 2008) for the Indian region to analyze the space–time structure of the monsoon rainfall. In this study, the summer monsoon rainfall from June to September (JJAS) is calculated for the period of 1960–2012. Five grids are equally weighted averaged for each latitude and longitude in order to remove small-scale perturbation of ISMR.

The hindcasts of five state-of-the-art coupled dynamical models are derived from the ENSEMBLES project (Weisheimer et al. 2009), including models from the Euro-Mediterranean Center for Climate Change (CMCC-INGV), European Centre for Medium-Range Weather Forecasts (ECMWF), the Leibniz Institute of Marine Sciences at Kiel University (IFM-GEOMAR), Météo France (MF), and UK Met Office (UKMO). The hindcasts used in this study were initiated from May 1st that yield 1-month-lead JJAS forecast for the period of 1960–2005. MME prediction is made by simply average of the five models' ensemble mean anomalies after removing their own climatology.

Sea surface temperature (SST) and sea level pressure (SLP) field are used to select predictors. The SST dataset used in this study is Extended Reconstructed Sea Surface Temperature (ERSST, v3b) from National Oceanic and Atmospheric Administration with 2° spatial resolution for the period 1960–2012 (Smith et al. 2008). The gridded 2.5° × 2.5° global monthly SLP data are derived from NCEP/NCAR reanalysis dataset (Kalnay et al. 1996) for the same period. We also used wind at 850 hPa from NCEP/NCAR reanalysis dataset to detect the circulation pattern. The twentieth century (20C) merged statistical analyses of historical monthly precipitation anomalies reconstructed data at 2.5° spatial resolution for the period from 1960 to 2005 are used to analyze global precipitation

(Smith et al. 2010). This dataset shows great similarity with IMD precipitation data over India.

2.2 Predictable mode analysis approach

A Predictable Mode Analysis (PMA) method is used to estimate potential predictability of climate variability (Wang et al. 2007; Lee et al. 2011, 2013; Wang et al. 2015a; Xing et al. 2014). The predictable modes are determined by the following criteria: (a) they represents major patterns of climate variability in the predictand field and ideally they are statistically separable from other higher modes; (b) the dynamical origins of these modes can be reasonably well understood, and (c) the dynamic models or/and P–E models are capable of predicting these modes with significant skills. Assuming that the predictable modes can be predicted perfectly, the potential predictability can then be estimated by the fractional variance accounted for by the predictable modes.

2.3 Selection of physical predictors in the P–E models

In the P–E models, predictors are selected primarily based on understanding of the physical linkages between the predictors and predictand. Correlation maps between each PC and the lower boundary variables (SST and SLP only) before June are used to identify potential predictors. Rather than "fishing" predictors as done in statistical models, we search only two types of precursory conditions. One is persistent signal defined as April–May mean. Normally the persistent predictors represent the "current" conditions right before the prediction period. It is hoped that the slow variation at the lower boundary will "persist" into next season similar to the persistent forecast. The persistent signal often signify the maintenance of the lower boundary anomalies that may be caused by local atmospheric-ocean interaction. This late spring (April–May) precursory condition would help to overcome the "spring barrier" of seasonal forecast (Wang et al. 2015b). Another is tendency signal from December–January to April–May (long-term tendency) or from March/April to May (short-term tendency). The tendency signal may reflect the direction of subsequent evolution. The selected predictors should reflect the physical processes that can explain the lead–lag relationship between the predictors and predictand, which will be illustrated in detail in Sect. 4. Domains of the selected predictors only maximize the correlation on the areas where they have clear physical meaning. Step-wise regression is used as an auxiliary tool to confirm the statistical significance of the predators-predictand correlation and to ascertain the mutual independence of the predictors. All predictors were selected with Fisher's F-test at the significance level of 0.05.

2.4 Three validation methods

2.4.1 Cross-validated reforecast

Leave-five-out cross validation (Geisser 1975; Blockeel and Struyf 2003) is used to validate the reforecast skill. Five years (validated sample) are withheld from the training sample and the regression coefficients are computed without them. These regression coefficients are used to forecast all 5 years. Then the process is repeated for all the other years to get the cross-validated reforecast for the period of 1960–2005.

2.4.2 Independent forecast

For independent forecast, the step-wise regression model is built using the data from a training period, no "future" information beyond the training period are utilized. Here we use regression model built for the period of 1960–2005 to make independent forecast for ISMR variability in 2006–2012.

2.4.3 Rolling-retrospective forecast

Progressional prediction models are built for rolling-retrospective forecast. Each progressional regression model is built by selecting 2 or 3 predictors from the predictor pool with stepwise regression and only 20-year training data. For example, the first prediction model is built for the training period of 1960–1979 to forecast ISMR in the next 10 years (1980–1989), and then the second prediction model is built using the 1970–1989 data to forecast the next 10 years (1990–1999). Totally, 4 segments of 10-year prediction are made for the 33-year retrospective forecast from 1980 to 2012 (the last prediction equation predicts only 3 years). The progressive retrospective forecast is considered as "independent forecast" in the sense that no "future" data were used in building the prediction equations. Note that the predictors and prediction equations for each progression prediction model are different because the training periods are different. However, the prediction skills for 1980–2005 may be inflated (Delsole and Shukla 2009) because the initial pool of predictors was first determined using the data of 1960–2005.

3 Predictable mode analysis and predictability of ISMR

3.1 Major patterns of the interannual variability

To investigate the patterns of ISMR variability, we performed an EOF analysis of the June–July–August-September

(JJAS) mean rainfall field over India for the period of 1960–2005, during which we have dynamical models' hindcast.

Figure 1a shows that the first EOF (accounting for 31.7 % of the total year-to-year variance) covers a large part of India with a uniform sign of anomalies. The second EOF (contributing 10.7 % of total variance) features a north–south dipole pattern. The negative loading is observed over Gangetic Plain while the positive loading is over Peninsular India. The third EOF accounts for 8.8 % of the total variance with heavy positive loading

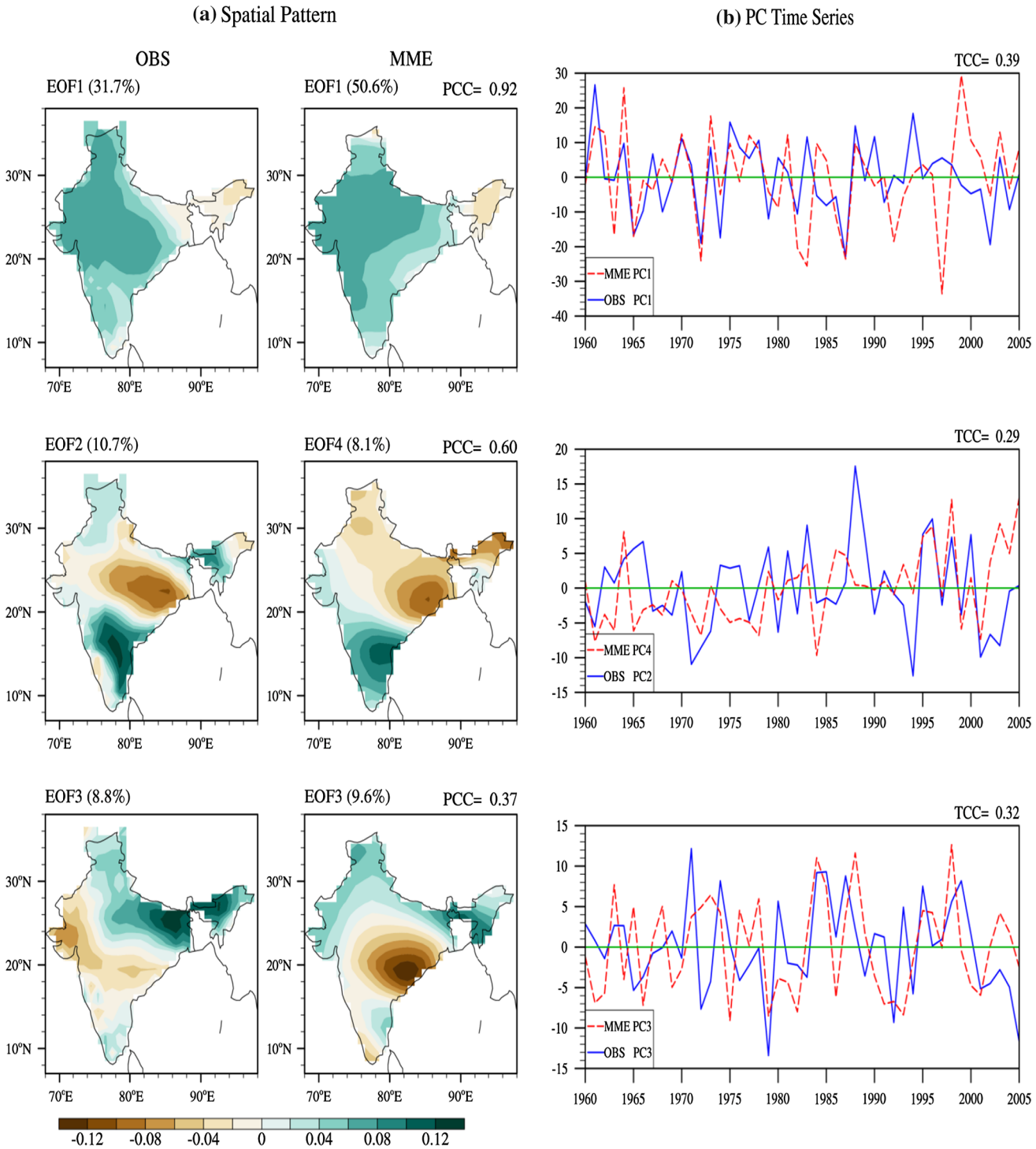

Fig. 1 **a** Spatial pattern and **b** corresponding time series of PC of three EOF modes of ISMR during the period of 1960–2005. Obtained from observation and hindcast from five coupled model's multi-model ensemble (MME) initiated from May 1st

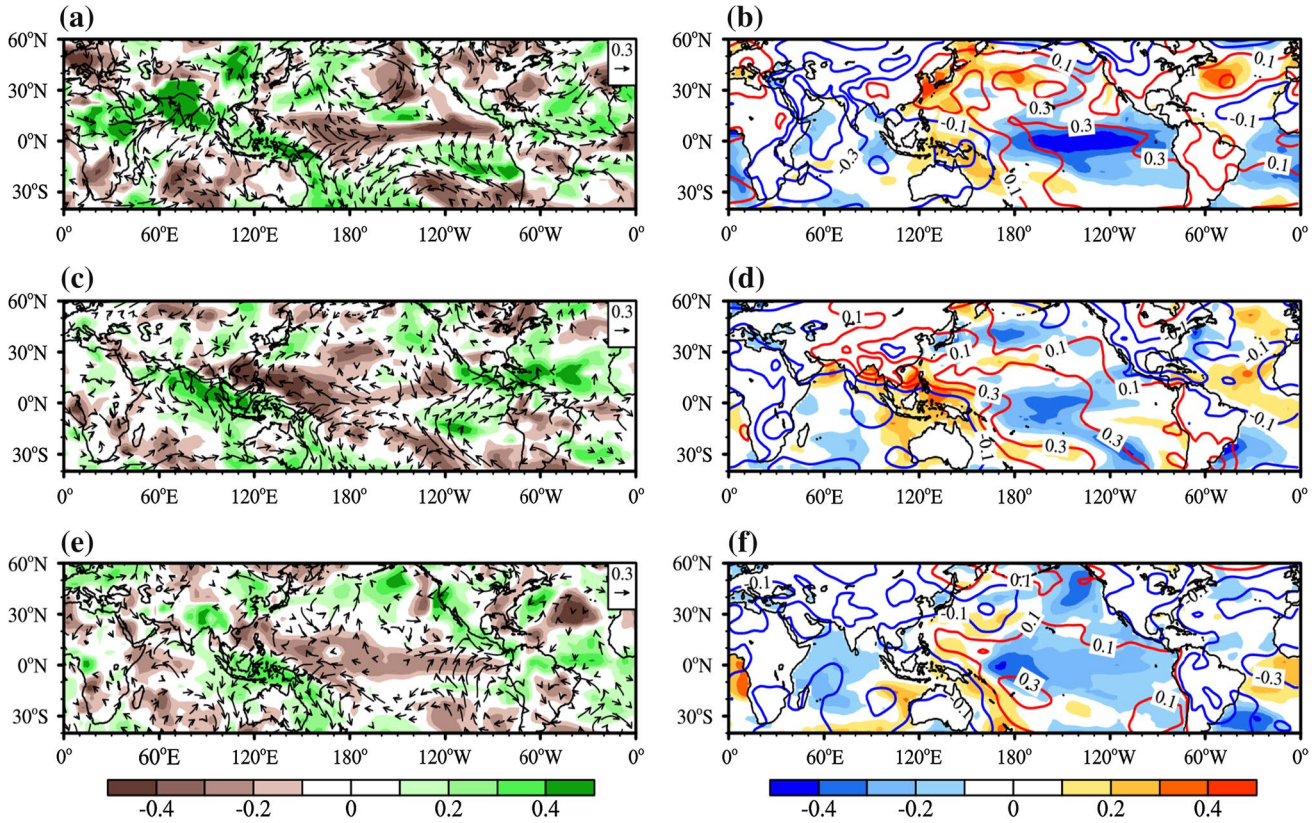

Fig. 2 Simultaneous (JJAS) correlation fields between PC1 and **a** precipitation (*shading*), 850 hPa wind, **b** SST (*shading*) and SLP (*contours*) for the period of 1960–2005. **c**, **d** are same as (**a**) and (**b**), respectively, but for PC2. **e**, **f** are same as (**a**) and (**b**), respectively, but for PC3

located along the north of Gangetic Plain and northeastern India and light negative loading to the western and central India.

3.2 Physical interpretation of the major patterns

Are these empirical patterns physically meaningful? Let us explore the dynamical origins of the first three modes, i.e., understand the processes governing the variability of each mode by examining simultaneous large-scale lower boundary anomalies. Associated with EOF1, suppressed rainfall is mainly over the western Pacific and enhanced rainfall occuring over northern Africa and most part of India (Fig. 2a). The SST anomalies associated with EOF1 features significant cooling over the central and eastern Pacific, indicating a developing La Nina (Fig. 2b). The lead–lag correlation of equatorial SST anomalies with reference to PC1 shows that the La Nina event starts from the eastern Pacific (EP, or Nino-3 region; Figure not shown), thus it is originated from a developing EP type of La Nina.

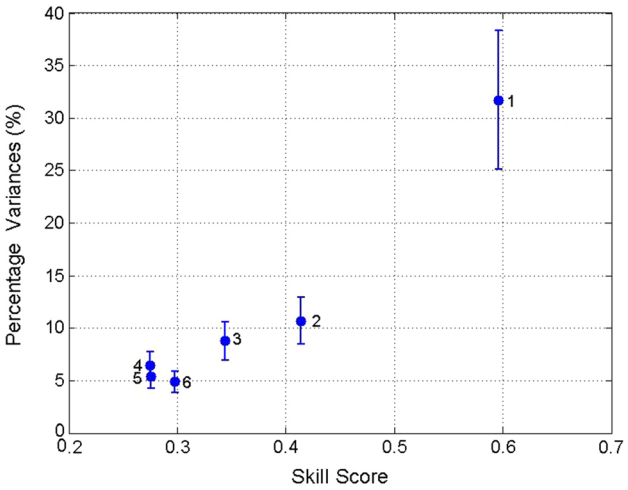

Fig. 3 Percentage variance (%) explained by the observed first six EOF modes (ordinate) and the combined forecast skill score for eigenvector (EV) and PC for each mode (abscissa). The skill score is defined by the square root of product of PCC score for EV and TCC score for PC time series for each mode. The *error bars* represent one standard deviation of the sampling error

The EP-La Nina induces east–west SLP seesaw with rising SLP over the Pacific subtropical highs in both hemisphere, and decreasing SLP over the eastern Hemisphere centered on the western Indian Ocean and Maritime Continent accompanied by strong cross-equatorial flows and intensified southwesterly monsoon over Arabian Sea, leading to an increase of ISMR over the entire India (Fig. 2a, b).

The precipitation anomalies associated with EOF2 (Fig. 2c) are similar to the first EOF pattern of Asian summer monsoon rainfall (Wang et al. 2015a) with suppressed rainfall over the Philippine Sea-equatorial western Pacific and enhanced rainfall over the maritime continent, south of India as well as two branches of tropical northern and southern Indian Ocean. The simultaneous SST anomalies related to EOF2 are characterized by a moderate cooling in the equatorial central Pacific (Nino3.4 region), which may be considered as a developing weak central Pacific (CP) type of La Nina; meanwhile, a strong warming occurs over the Western Pacific and northern Bay of Bengal and Arabian Sea as a result of the enhanced western Pacific subtropical High (Fig. 2d). This SST pattern is also similar to that associated with EOF1 of Asian summer monsoon rainfall (Wang et al. 2015a). The high SLP anomalies are located over the central Pacific, which extend northwestward into Philippine Sea and south Asia, causing suppressed rainfall over northern India (Mishra et al. 2012). Meanwhile, the enhanced convection over the southern Maritime Continent induces a cyclonic circulation anomaly extending from the Maritime Continent to southern India, which enhances the precipitation over southern India (Wang et al. 2003, 2015a).

The EOF3 is related to the enhanced rainfall over the Maritime Continent and southeast tropical Indian Ocean and suppressed rainfall over western tropical Indian Ocean (Fig. 2e). The precipitation anomaly and associated wind anomalies are consistent with equatorial Indian Ocean

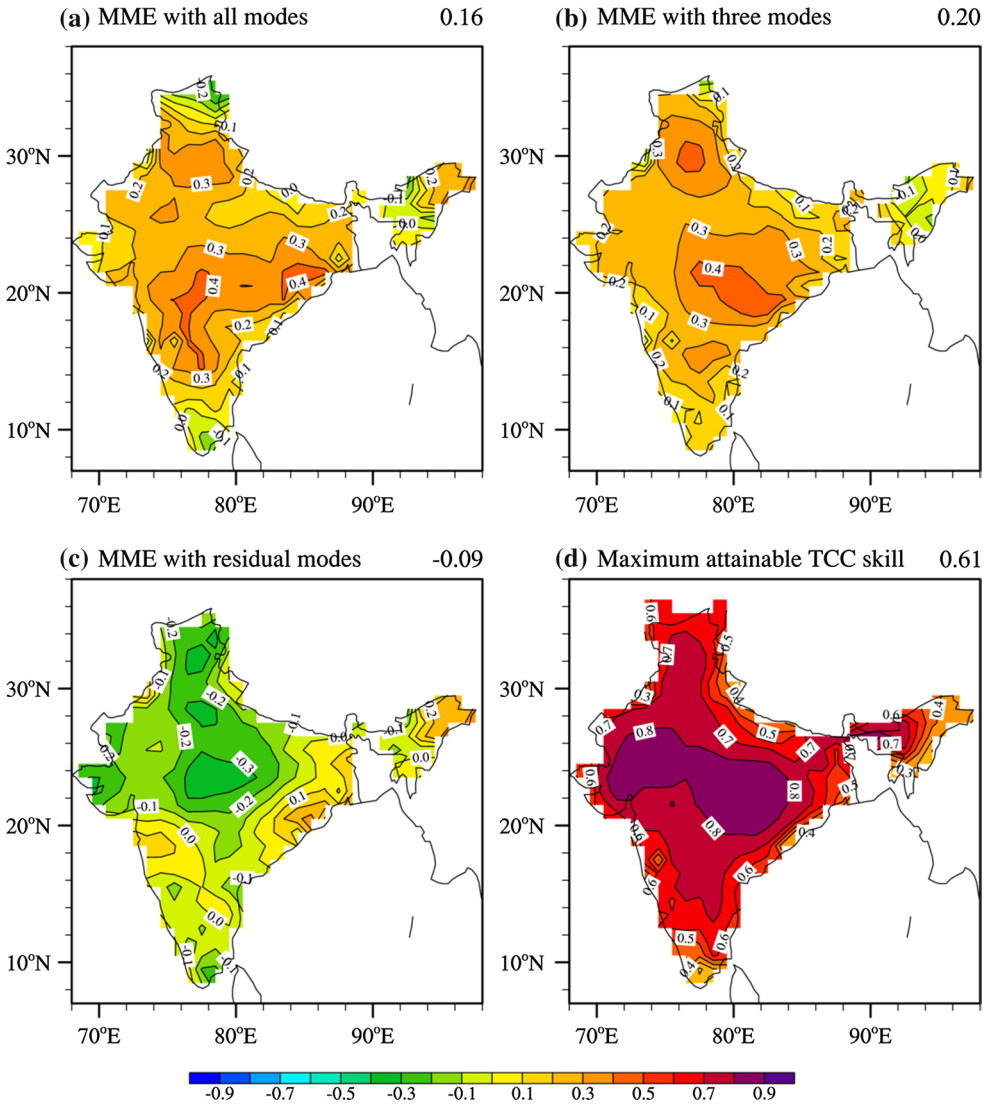

Fig. 4 The MME's temporal correlation coefficient (TCC) skills for ISMR prediction obtained by using, **a** all EOF modes, **b** three predictable modes and **c** all the rest modes for 1960–2005, **d** The maximum attainable TCC skills from the first three predictable EOF modes. The maximum attainable TCCs are measured by the TCC between the observed total field and the observed predictable components of the field. The *number* in the *right upper* corners indicates averaged correlation skills over India

Oscillation (EQUINOO) in precipitation (Gadgil et al. 2004). The SST anomalies with reference to EOF3 show a weak cooling near the dateline, which enhances convection over the northern Maritime Continent. The enhanced convective heating then induces a cyclonic anomaly over the northern Bay of Bengal and northern India (Fig. 2f), suggesting a favorable condition for the convection over north of Gangetic Plain and northeastern India. Therefore, the dynamical origins of these three modes can be well distinguished and their teleconnection patterns can be reasonably understood.

3.3 Identification of the predictable modes

Are these three modes predictable? One way to address this question is to examine whether the coupled climate models can simulate or predict them. We took five ENSEMBLE models' MME hindcast results from 1960 to 2005 and made an analysis parallel to the observed data analysis. Figure 1 compares the observed and model predicted major modes of variability. We find that the first three observed modes correspond, respectively, to the first, fourth and third MME-predicted EOF modes in terms of their similarities in spatial patterns and correlations with principle components. The MME tends to underestimate the variance of the second observed mode. The pattern correlation coefficient (PCC) skills of spatial patterns and the TCC skill of the principal component (PC) of the MME are presented for each mode in Fig. 1. Note that the MME can capture the spatial distribution of the first two observed modes but has remarkable spatial errors for the third mode over eastern India. The number of grids over the whole India is 357. Taking account of spatial correlations, assuming the degree of freedom is reduced to 35 (about 10 % of total sample size), the PCC skill of 0.34 is significant at 95 % confidence level. Overall, however, the MME offers significant skills (Fig. 1) in predicting the first three observed EOF patterns with PCC skills higher than 0.34 and TCC skills exceed 0.29 (95 % confidence level). Those are criteria used to determine predictability of the modes.

To see whether these three modes are separable from other higher modes, we examine their fractional variance contributions and the skills of the MME in capturing these modes. The results are presented in Fig. 3. Here the ordinates denotes the fractional variance explained by the observed EOFs along with the range of the uncertainty due to sample errors (North et al. 1982). The abscissa represents the MME's skill score in predicting each observed EOF mode. The skill score (Lee et al. 2011, 2013) is defined by the PCC score for eigenvector and TCC score for PC time series, which is calculated by

$$\text{Skill Score} = \sqrt{PCC \times TCC} \quad (1)$$

Table 1 The definitions of predictors

Predictor	Definition
PC1a	May minus April N–S SST dipole: SST (10°S–50°S, 175°E–150°W) minus SST (0°N–25°N, 180°–140°W)
PC1b	April–May minus December–January SST (40°S–40°N, 145°E–80°W) averaged over the western Pacific K-shape area minus eastern Pacific triangle
PC1c	May minus March SST averaged over (10°S–30°S, 60°E–125°E)
PC2a	April–May mean SLP averaged over (40°S–15°N, 155°E–130°W)
PC2b	April–May minus December–January SST averaged over (20°S–5°S, 100°E–160°E)
PC3a	April–May mean SLP averaged over (10°N–40°N, 175°–140°W) and (30°S–55°S, 160°E–150°W)
PC3b	April–May mean SLP averaged over (30°N–45°N, 25°W–10°E) minus (50°N–70°N, 10°W–20°E)

We use the grids in the defined region which correlation coefficients with corresponding PC are significant at 95 % confidence level

Table 2 The correlation coefficients between each PC and corresponding predictors and among each other during the period of 1960–2005

	PC1	PC1a	PC1b	PC1c
PC1a	**0.59**		0.27	*−0.32*
PC1b	**0.54**	0.27		**−0.51**
PC1c	**−0.58**	*−0.32*	**−0.51**	
	PC2		PC2a	PC2b
PC2a	**0.49**			*0.34*
PC2b	**0.49**		*0.34*	
	PC3		PC3a	PC3b
PC3a	**0.57**			*0.35*
PC3b	**0.57**		*0.35*	

The bold (italic) numbers denote statistically significant at 99 % (95 %) confidence level

Note that the first EOF mode is clearly distinct from the other EOF modes; the second and third EOFs are, to a certain extent, separated from other higher modes. Due to short record, the observed EOF2 and EOF3 are not statistically separable due to sample error (Fig. 3). In this case, it is possible that the order of model predicted EOFs is different with observed EOFs (Lee et al. 2011), because the dynamical model may capture these EOF modes with different fractions of explained variance. Moreover, the first three observed EOF modes are reasonably predicted by the MME with higher fidelity (skill scores) than the other modes. The PCC skills of first three predicted EOF patterns and TCC skills of corresponding PC are significant at 95 %

confidence level (PCC > 0.34, TCC > 0.29), so here the skill score of 0.32 is considered as having significant skill. Thus, the first three observed modes are distinctive from the rest higher modes that are likely unpredictable.

The above analysis suggests that the first three observed modes of ISMR variability may be potentially predictable while the other modes seem to have little predictability. To further test this assertion, we compare the TCC skills made by the MME prediction using the identified three predictable modes and using all modes (i.e., the original predicted field). For the 3-mode MME prediction, the predicted field is reconstructed by using the spatial structures of three predicted modes multiplied by their correspondingly predicted PCs. The area-averaged TCC skill averaged over the entire India by using all modes and by using only the three modes are, respectively, 0.16 and 0.20 for the 46-year period of 1960–2005 (Fig. 4a, b). Note that all residual modes (the modes other than the three) make little contribution to the prediction skill (Fig. 4c). Thus, the prediction skill for ISMR mainly lies in the skills for prediction of these three predictable modes. The results here suggest that the first three modes are source of the prediction skill in dynamical model MME.

3.4 Potential predictability of the ISMR anomaly pattern

The predictable mode analysis suggests that the first three observed modes can be regarded as the predictable modes for ISMR. The first three EOF modes together account 51.2 % of total variance in the observation. If we assume these modes can be perfectly predicted, the total fractional

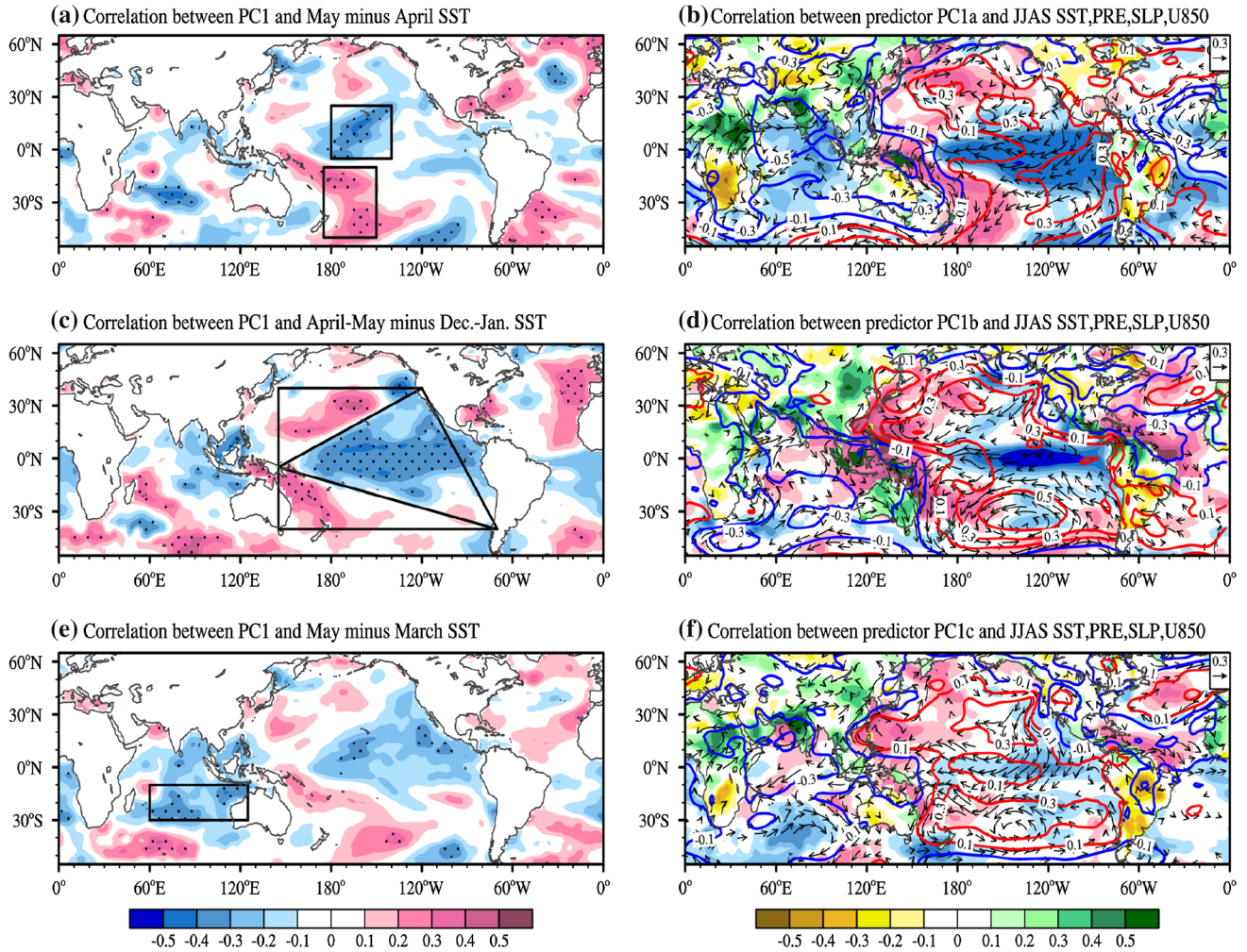

Fig. 5 The correlation maps between PC1 and **a** May-minus-April SST, **c** April–May minus December–January SST and **e** May minus March SST. The *box regions* show the locations of predictor for PC1a, PC1b and PC1c in (**a**), (**c**) and (**e**), respectively. *Dotted areas* denote regions with correlation coefficients significant at 95 % level. **b** Correlations between predictor PC1a and the JJAS SST over ocean (*shading* with *blue* to *red*), precipitation over land (*shading* with *yellow* to *green*), SLP (*contours*) and 850 hPa winds (vectors) during 1960–2005. **d**, **f** are same as (**b**), but for predictor PC1b and PC1c, respectively

variance accounted for by the predictable modes can be used to estimate the upper limit of the potential predictability. Based on this analysis, about one half of the ISMR seasonal variability is predictable.

The potential predictability can also be measured by the TCC between the observed total field and the observed predictable components of the field (Lee et al. 2011, 2013). Figure 4d shows the spatial distribution of the maximum attainable TCC skill during the period of 1960–2005. The area-averaged maximum attainable TCC skill over the whole India is 0.61. Relatively high skill appears in the central India. In general, there is still a large room to improve the ISMR prediction via improvement of the model and better reproducing the first three modes.

4 The ISMR anomaly pattern prediction by P–E models

As we demonstrated above, the first three EOF modes may be predictable and the dynamical models have so far limited prediction skills. Therefore, we want to build P–E models for predicting each PC of these three modes, with which we may further predict the spatial distribution of the rainfall anomalies by using the 3-mode reconstruction.

4.1 Searching for physical meaningful predictors

The simultaneous large-scale anomalies (Fig. 2) associated with each PC also provide dynamical insight for selecting physically meaningful predictors. For each PC of the ISMR, two or three predictors are selected for construction of P–E prediction model. These predictors stand for different precursory lower boundary forcing on the monsoon circulation system. The principles and methods of selection predictors have been described in Sect. 2. All predictors (their definitions are summarized in Table 1) have high TCC (significant at 0.99 confidence level) with the corresponding PCs (Table 2). The variance that explained by these predictors for corresponding PC can be reflected by the prediction skill of cross-validated reforecast. These predictors are selected because of their physical meanings and are relative independent from each other, which are explained in the next few paragraphs.

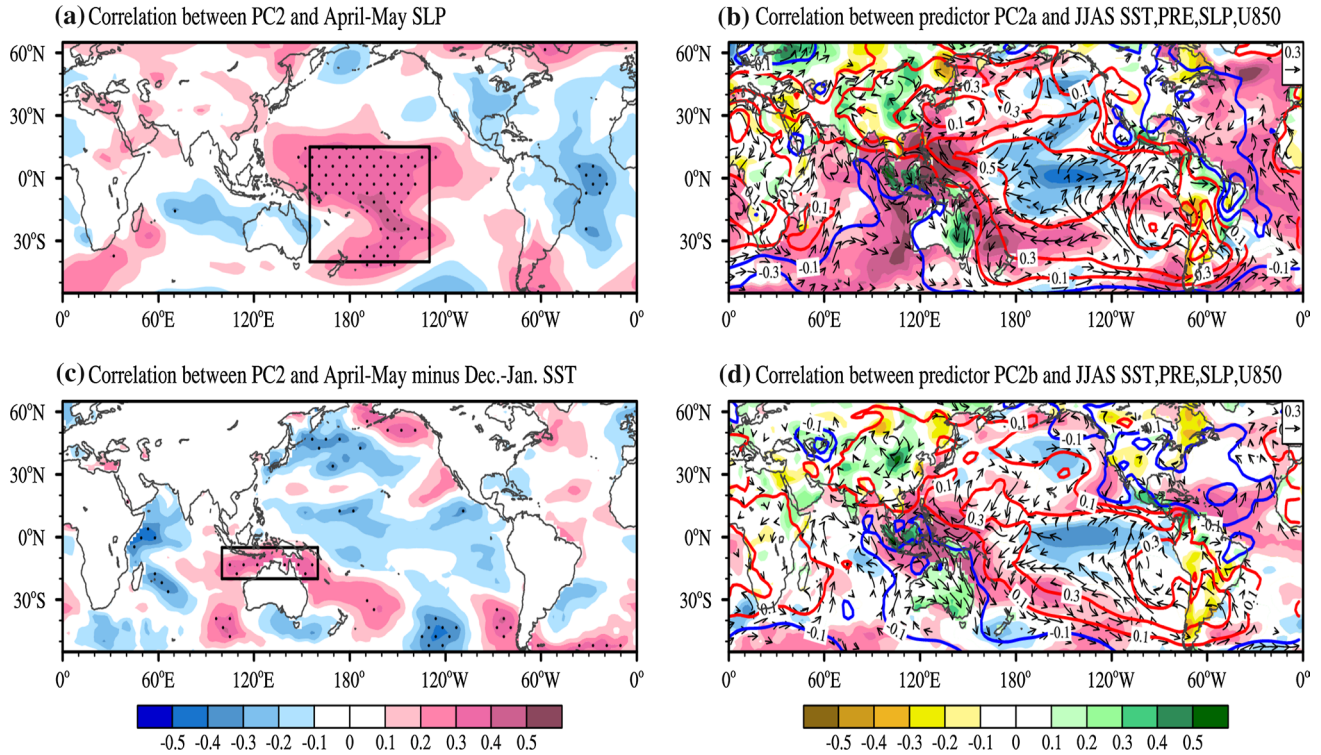

Fig. 6 The correlation maps between PC2 and **a** April–May mean SLP and **c** April–May minus December–January SST. The *box regions* show the locations of predictor for PC2a and PC2b in (**a**) and (**c**), respectively. *Dotted areas* denote regions with correlation coefficients significant at 95 % level. **b** Correlations between predictor PC2a and the JJAS SST over ocean (*shading* with *blue* to *red*), precipitation over land (*shading* with *yellow* to *green*), SLP (*contours*) and 850 hPa winds (vectors) during 1960–2005. **d** is same as (**b**), but for predictor PC2b

For PC1, all three predictors (PC1a, PC1b and PC1c) are derived from SST tendency fields, i.e., SST tendency predictors. The persistent-type SST predictors and the SLP predictors are also examined but not selected because of their dependency on the selected three. The predictor, PC1a, is a short-term tendency of dipole SST with cooling in the northern central Pacific and warming in the southern central Pacific from April to May (Fig. 5a). This north–south dipole SST tendency implies a building up meridional thermal gradients that can strengthen equatorial easterlies and westward surface currents, leading to a central-eastern Pacific cooling in JJAS (Fig. 5b), which enhances ISRM through changing Walker circulation (Kumar et al. 2006). Predictor PC1b denotes an east–west contrast in the SST tendencies, i.e., the central-eastern Pacific triangle SST cooling and K-shape Pacific SST warming from winter to spring (Fig. 5c). This dipole tendency foreshadows enhanced subtropical Highs in both the North and South Pacific, associated equatorial cooling in the ensuing summer and the associated trade winds cause moisture convergence over the Asian monsoon region (Wang et al. 2013), and thus contribute to intensification of ISMR (Fig. 5d). In addition, the cooling SST tendency from March to May in the southern Indian Ocean (predictor PC1c, Fig. 5e) intensifies the land-sea thermal contrast during summer and the associated southwest monsoon with large amount water vapor transporting to India (Fig. 5f).

For PC2, only two independent predictors are selected, one is persistent SLP and the other is SST tendency. The first predictor, PC2a, represents the high SLP anomalies located at the central and southern Pacific in April and May (AM) (Fig. 6a). The enhanced SLP induces CP-La Nina type of anomalous cooling which generates, through suppressing convection, a strong anti-cyclonic anomaly over the western tropical Pacific. As can be seen in Fig. 6b, the strengthened West Pacific Subtopic High extends to the foothill of Himalayas, leading to reduced rainfall over northern India and enhanced rainfall south of the anti-cyclonic ridge. The second predictor, PC2b, signifies a SST warming tendency at southern Maritime Continent from northern winter to spring (Fig. 6c), which leads to enhanced rainfall over the Maritime Continent, further generating low-pressure anomalies extending to southern India by Rossby wave emanation (Wang et al. 2013; Fig. 6d), which intensifies the rainfall there. The predictor PC2b is also a precursor for a CP-type La Nina.

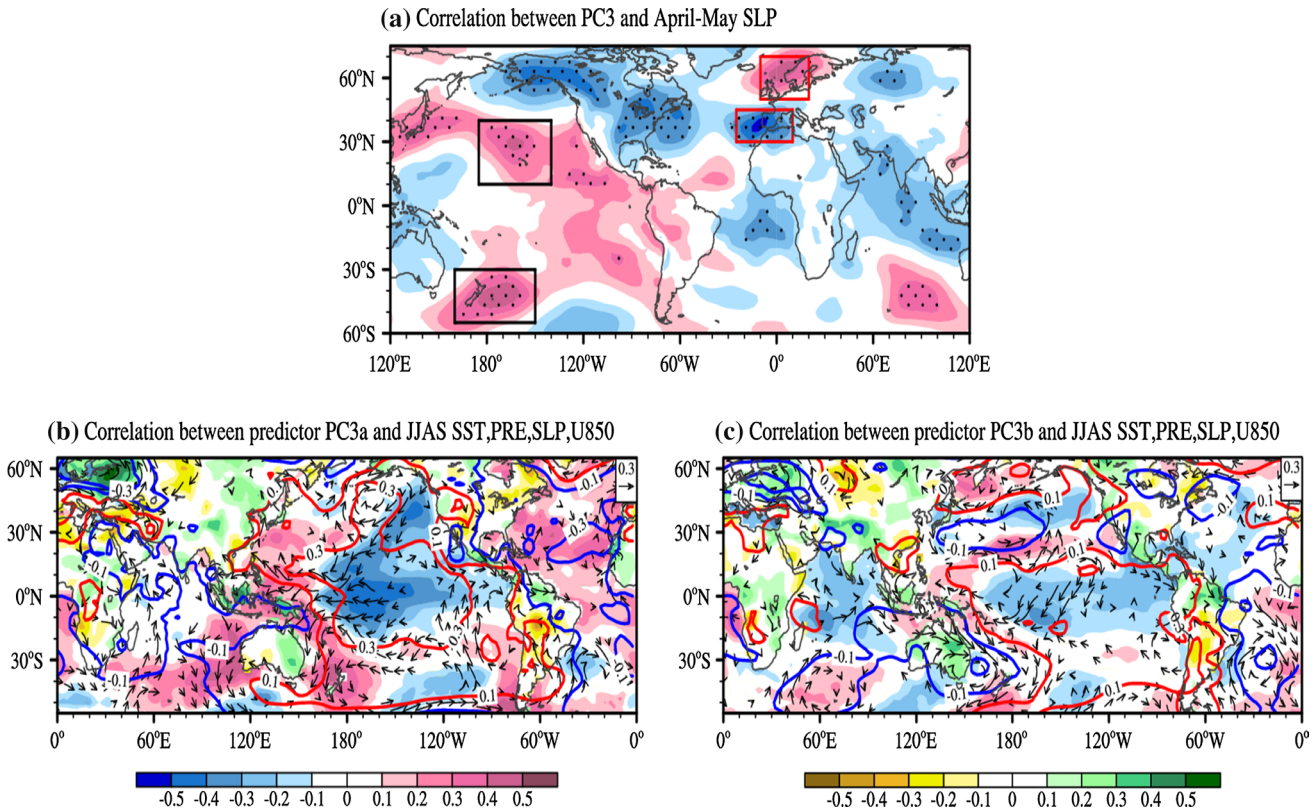

Fig. 7 The correlation maps between PC3 and **a** April–May mean SLP. The *black* and *red* box regions show the locations of predictor for PC3a and PC3b, respectively. *Dotted areas* denote regions with correlation coefficients significant at 95 % level. **b** Correlations between predictor PC3a and the JJAS SST over ocean (*shading* with *blue* to *red*), precipitation over land (*shading* with *yellow* to *green*), SLP (*contours*) and 850 hPa winds (vectors) during 1960–2005. **c** is same as (**b**), but for predictor PC3b

For PC3, only two predictors are found in April–May (AM) mean SLP (persistent type); the precursory condition in SST field is weak. The ISMR links to summer EQUINOO in precipitation. But the corresponding precursor in spring is weak, so that the related predictor is not able to be selected for EOF3. As seen in Fig. 7a, the first predictor, PC3a, denotes an intensified Northern Subtropical High and rising pressure in the southwest Pacific in AM. This SLP pattern leads to enhanced easterlies and SST cooling in the equatorial central Pacific near the dateline in the ensuing summer (Fig. 7b). The cooling SST anomalies enhance the precipitation over the northern Maritime Continent. The heating from the northern Maritime Continent can excite a cyclonic anomaly Rossby wave response over the northern Bay of Bengal and northern India (Gill 1980). Over India, the 20C reconstructed precipitation does not show EOF3 precipitation pattern, but if we use IMD precipitation data the regressed precipitation pattern does resemble the EOF 3 pattern, suggesting the data uncertainty in the EOF 3 mode. The second predictor PC3b is a SLP dipole in AM over Western Europe (Fig. 7a). This dipole seems to extend southeastward, resulting in a low pressure extending from Scandinavia to northwest India (Fig. 7c). Under this circulation background, Himalayan orographic forcing may also play an important role in modulating the rainfall over northeast of India (Sinha et al. 2014).

4.2 The hindcast skills of the P–E prediction model

Based on the abovementioned arguments, we consider these selected predictors physically meaningful. A set of stepwise regression prediction equations is established for each PC using the corresponding selected predictors. Table 3 shows three types of validation skills (see Sect. 2 for details) for each PC in term of TCC. The cross-validated reforecast and rolling-retrospective forecast both show significant TCC skills at 99 % confidence level. For PC1, the cross-validated reforecast skill for 46 years (1960–2005) is 0.71. The independent forecast for the recent 7 years (2006–2012) yields a TCC of 0.80. For the rolling-retrospective forecast, the skill is 0.66 during period of 1980–2012. The forecast skill for PC2 and PC3 are also reasonably well. The validated TCC skills suggest that the P–E models have good capacity to predict the first three PCs.

As shown by the red dashed line in Fig. 8, the MME predicts the first three PCs with significant skill (95 % confidence level) of 0.39, 0.29 and 0.32, respectively. The cross-validated predicted PCs (blue line in Fig. 8) by the P–E models are capable of capturing the interannual variation of observed PCs with much higher TCC skills of 0.71, 0.56, and 0.63, respectively. The P–E model prediction skill using the first three PCs also achieved the acceptable level (0.29 for 95 % confidence level) for predictable modes.

Table 3 The prediction skills (correlation coefficients) from P–E models for each PC

	PC1	PC2	PC3
Cross-validated reforecast (1960–2005)	**0.71**	**0.56**	**0.63**
Independent forecast (2006–2012)	*0.80*	*0.82*	0.47
Rolling-retrospective forecast (1980–2012)	**0.66**	**0.59**	**0.53**

The bold (italic) numbers denote statistically significant at 99 % (95 %) confidence level

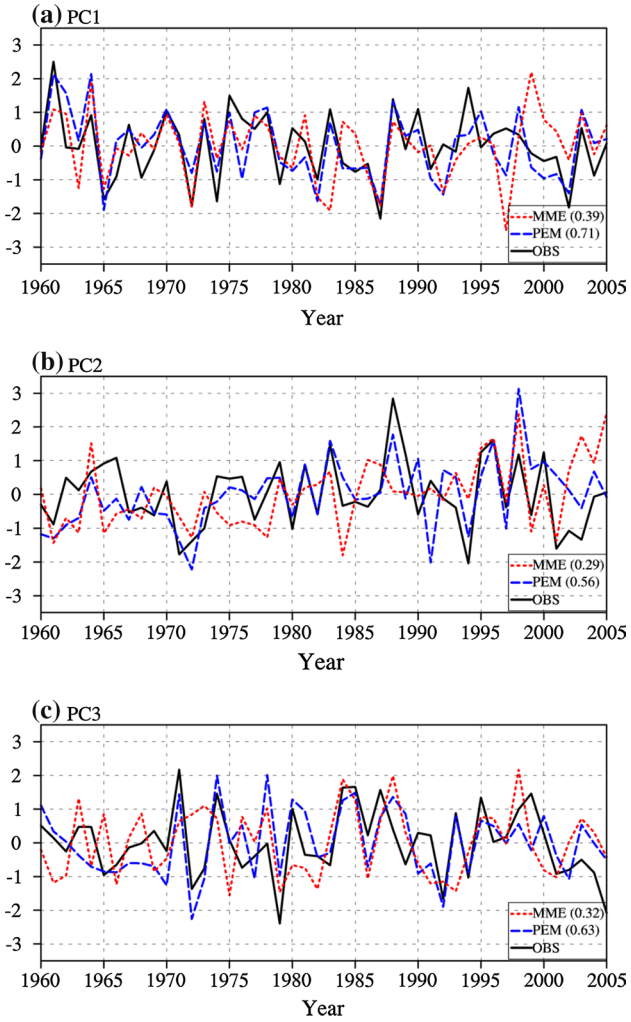

Fig. 8 The corresponding PC of the first three EOF modes (**a**–**c**) in observation (OBS), P–E model (PEM) cross-validated prediction and Multi-Model Ensemble (MME) dynamical prediction from 1960 to 2005. The *numbers* within the *parenthesis* in the figure legend indicate the TCC between the observed and predicted PC

Predicted ISMR precipitation anomaly pattern can be reconstructed by the sum of the first three predicted PCs multiplied by their corresponding observed EOF patterns. The TCC between predicted and observed rainfall anomalies are calculated for each grid and the result is shown

in Fig. 9. The cross-validated reforecast skills during the period of 1960–2005 are greater than 0.4 (exceeding 99 % confidence level) over most parts of India (Fig. 9a). For independent forecast (2006–2012), higher TCC (0.5–0.7) are found over Deccan Plateau, while lower TCC occurred in eastern Gangetic Plain (Fig. 9b). For the rolling-retrospective forecast (Fig. 9c), the northern, eastern and central India have better skills with TCC greater than 0.5 during the period of 1980–2012. The area-averaged TCC skill over the entire India is 0.43, 0.37 and 0.35, respectively, for the cross-validated reforecast, independent forecast and rolling-retrospective forecast. Note that the independent and rolling-retrospective forecast skills of PC3 are lower than the cross-validated reforecast skill (Table 3). The third EOF mode mainly stands for rainfall anomaly over north of Gangetic Plain and northeastern India. Thus, the TCC skills over north central India for rolling-retrospective forecast (Fig. 9b) and independent forecast (Fig. 9c) are lower than cross-validated reforecast (Fig. 9a).

In order to further estimate the year-to-year variation of the prediction skills of rainfall pattern. We compare the time series of the PCC skill obtained by the P–E models, the three-mode MME forecast and the potential attainable forecast skill using the perfect prediction of the 3 predictable modes in Fig. 10. The PCC skill shows large year-to-year variation for the predictions made by the P–E models and the MME. The long-term mean PCC skills of P–E models and the three-mode MME are 0.35 and 0.22, respectively. The P–E prediction shows superior PCC skill. It is note that the PCC skills of the P–E model and MME are both close to the attainable prediction skill in some years such as 1961, 1964, 1972, 1975, 1982 and 2002. In general, both the P–E prediction and the MME prediction have higher skills when the attainable skill is higher. However, both predictions have no skill in some years including 1962, 1963, 1967, 1976, 1980, 1989, 1997 and 2001.

There are a number of factors affecting PCC skills of prediction by P–E model or MME. One is to what extent the

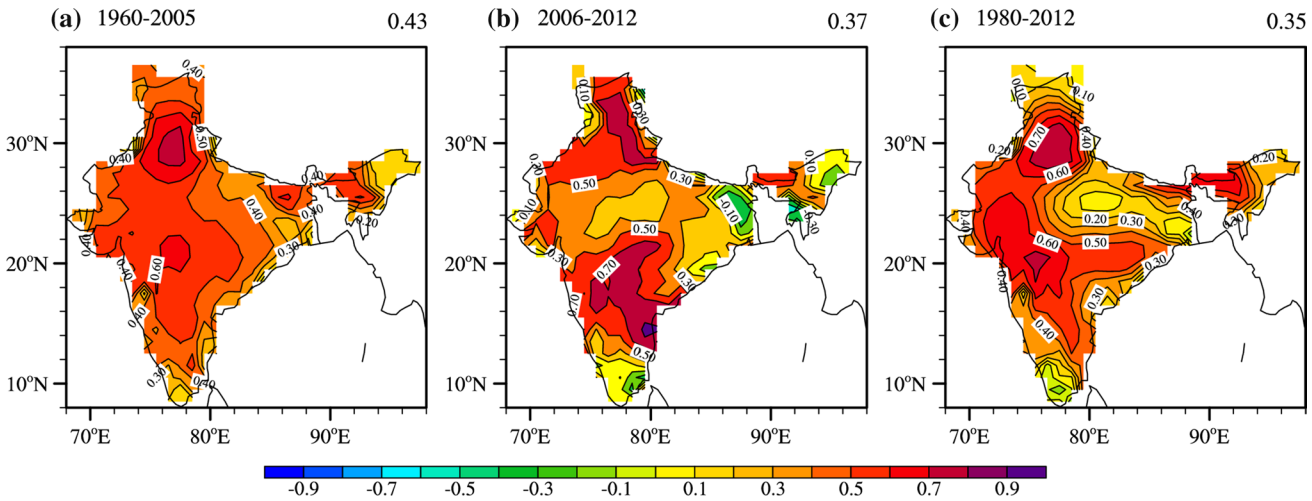

Fig. 9 The TCC skills of **a** cross-validated reforecast, **b** independent forecast and **c** rolling-retrospective forecast for each grid in India obtained from P–E model. The *number* in the *right upper corners* indicates averaged TCC over India

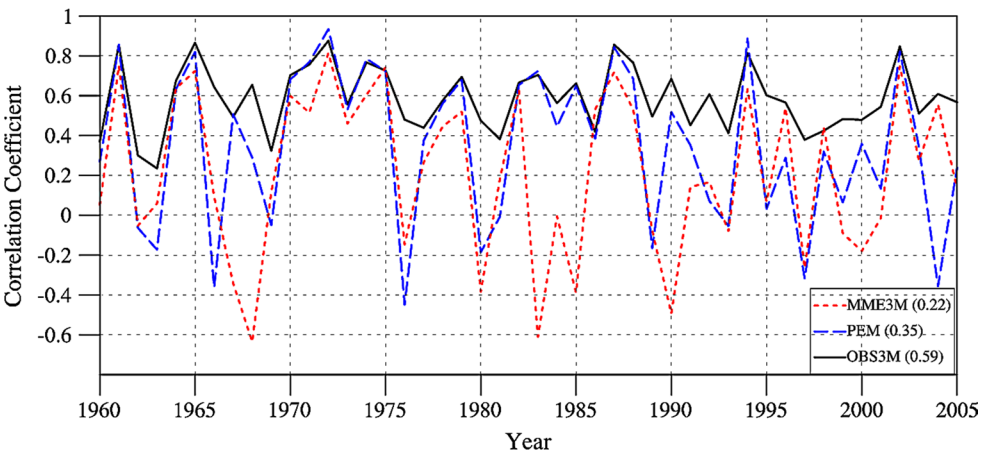

Fig. 10 The PCC skill for ISMR prediction as a function of forecast year using cross-validated P–E model prediction (PEM), prediction with the MME's 3 modes (MME3M) and potential attainable forecast skill using observed 3 modes (OBS3M). The *numbers* within the *parenthesis* in the legend indicate the averaged PCC skill

Table 4 Prediction skills of all Indian rainfall index (AIRI) made by P–E model and MME (derived from all modes and 3 modes) during the period of 1960–2005 and 1980–2005

	P–E model[a]	P–E model[b]	MME	
1960–2005	**0.67** (cross-validated reforecast)	**0.72** (cross-validated reforecast)	**0.43** (all modes)	**0.41** (3 modes)
1980–2005	*0.44* (rolling-retrospective forecast)	**0.65** (rolling-retrospective forecast)	0.18 (all modes)	0.14 (3 modes)

The bold (italic) numbers denote statistically significant at 99 % (95 %) confidence level

[a] Building for direct prediction of AIRI (Wang et al. 2015b)

[b] Building from predictable modes

predictable EOF modes can represent the actual rainfall pattern in an individual year. The PCC skills of the 3 observed modes (OBS3M) reflect the overall extent that predictable modes represent the actual rainfall pattern. However, their representativeness varies with years. When these predictable modes are not dominant in an individual year, even if the prediction for PCs is perfect, it contributes little to the prediction of actual rainfall pattern. That is the reason why the PCC skills of P–E model or MME tend to be low or even negative when PCC skills of OBS3M are low. That also implies that some new modes need to be discovered, although they might not be captured by the dynamical models at this stage. Another factor is the prediction skill for each PC. When the PCC skills of OBS3M are higher, the PCC skills of P–E model and MME are mainly affected by their prediction skills of each PC. So improving prediction skill of each predictable PC is essential. Third, our selection of predictors are based on understanding of the lead–lag relationship, therefore the statistical skills are not necessarily high. It is pretty sure that one can get statistical predictors that have higher correlation skill. But such pure statistical fitting may inflate the prediction skill and may drop the skill in real prediction. This is precisely the P–E approach tried to avoid.

5 Conclusion and discussion

Major modes of ISMR have been extracted by conducting EOF analysis of the JJAS mean precipitation over India. The first three EOF modes account for 51.2 % of total interannual variance, or together they can explain over half of Indian summer rainfall variability. The first EOF mode represents a nearly uniform pattern across India. Second EOF mode is a north–south dipole rainfall pattern. Third EOF mode mainly stands for rainfall anomaly over north of Gangetic Plain and northeastern India.

Dynamical origins of the first three modes are explored by examining simultaneous large-scale lower boundary anomalies. The SST anomalies associated with EOF1, EOF2 and EOF3 are characterized by an EP-type La Nina, a CP-type La Nina, and a cooling center near dateline, respectively. These equatorial Pacific SST anomalies, while located in different longitudes, can all set up a specific teleconnection pattern that affects Indian monsoon and results in different rainfall EOF patterns. But are those modes predictable?

It is important to define criteria for considering a mode to be predictable. First, the criteria should be a function of variable because the predictability is a function of variable. Dynamical models have difficulty in capturing the land precipitation than other variables, so the explained variance by prediction is much lower than JJA 200-hPa GPH (Lee et al. 2011) or Asian winter temperature (Lee et al. 2013). Secondly, although prediction skill of MME for land precipitation is much lower than other variables, it should capture the major EOF patterns and PCs with statistical significant skills (say, 95 % confidence level). We show that the MME of five state-of-the-art ENSEMBLE dynamic models' 46-year (1960–2005) hindcast can reproduce the observed first three EOF of ISMR significantly (PCC > 0.34, TCC > 0.29). Thirdly, it is important to demonstrate that the dynamical prediction skill of MME for ISMR pattern mainly comes from the skills for the prediction using the predictable modes. As shown in Fig. 4, the MME predictions made by using all EOF modes and by these three modes only, yield area-averaged TCC skill of 0.16 and 0.20, respectively over entire India and for the period of 1960–2005, indicating that the MME's predictive skill mainly come from the prediction skill of these three modes. Fourthly, assuming the EOF pattern are perfectly captured (PCC = 1), the variance explained by prediction equals to (skill score)^4, i.e., (TCC)^2. This assumption is reasonable because the spatial pattern biases can be corrected by replacing the model EOF patterns by the observed EOF patterns as in Wang et al. (2015a) for Asian summer monsoon prediction. So the variance explained by prediction is determined by TCC skill of PCs. For this purpose, we simply assume the TCC must exceed the significance at 95 % confidence level.

Thus, the first three modes can be regarded as the predictable modes for ISMR. About one-half of the total observed variability is potentially predictable over India. The estimation of the predictability for ISMR patterns suggests that the current models still have large room for

improvement. Therefore, we developed Physics-based Empirical (P–E) model based on the understanding of monsoon dynamics and the lead–lag relationship between the predictors and predictand (PCs in this case). Physically meaningful predictors are selected for prediction of each PC and their linkages with ISMR are discussed. Prediction of ISMR anomaly patterns based on these physical-empirical predictors has a cross-validated reforecast skill with area-averaged TCC of 0.43, which is significantly better than the current dynamical models' MME skill (0.16) for the same period of 1960–2005. Even for the independent forecast during the period of 2006–2012, the skill only dropped slightly.

Although the present work focuses on prediction of the anomaly rainfall patterns, it would be interesting to see to what extent the P–E model can predict the AIRI compared with the dynamical models' MME prediction (Table 4). The cross-validated reforecast (rolling-retrospective forecast) skill of the P–E models yields a TCC skill of 0.72 (0.65) for the period of 1960–2005 (1980–2005). MME prediction shows lower skill of 0.43 (0.18) for the period of 1960–2005 (1980–2005). It is also interesting to note that the P–E model built specifically for direct prediction of AIRI (Wang et al. 2015b) yields a skill of 0.67 for cross-validated reforecast (1960–2005) and 0.44 for rolling-retrospective forecast (1980–2005). Therefore, the skills of direct prediction of AIRI are lower than the skills here built from predictable mode analysis especially during the period of 1980–2005, suggesting that the P–E models built from predictable modes (or for the anomaly pattern) can improve the AIRI prediction because it takes into account the regional distribution signals and involves more predictors. This new method also adds another independent forecast tool for AIRI.

Understanding the physical linkages between predictand and predictors are crucial for selecting predictors and for improving prediction skills. The principles of searching for relatively independent and complimentary predictors should be useful for reduction of the predictive skill drop (Wang et al. 2015b). While the causative processes linking the predictors and the major modes of the ISMR have been speculated, they are, by no means, rigorous proofs; thus, further well-designed numerical experiments are needed to validate or refuse the articulations proposed in the present study.

We should note that the 46-year retrospective cross-validated correlation skills shown in Fig. 8 are likely inflated because all the data (model development and validation) are used to select the predictors (Delsole and Shukla 2009). In addition, the predictors derived from the current 46 years of data for ISMR patterns may vary with time or experience secular changes. That is partially the reason why the predictor used for EOF1 of Asian summer monsoon rainfall (Wang et al. 2015a) derived from 32 years (1979–2010) are different from we selected for EOF2 of ISMR in this study, although these two EOF modes have similar characters.

The dominant EOF modes vary with the study period, so the total explained variance of predictable EOF modes may change and the predictable modes themselves may change accordingly. But the identified predictable modes must capture large part of the total variability, so that prediction can be useful. The modes identified here are only valid for the recent 46 years period. The selected predictors are by no means optimum. We anticipate that the established prediction equations will be useful for next few years, but continuous detection of secular changes and modifications of the predictors/prediction equations are imperative.

Acknowledgments This work was jointly supported by NOAA/MAPP Project Award Number NA10OAR4310247, the US National Science Foundation awards #AGS-1005599, the National Research Foundation (NRF) of Korea through a Global Research Laboratory grant (MEST, #2011-0021927) and the APEC Climate Center. We also acknowledge support from the US-China Atmosphere–Ocean Research Center sponsored by Nanjing University of Information Science and Technology (NUIST). This is publication No.9451 of the School of Ocean and Earth Science and Technology, the publication No.1129 of the International Pacific Research Center and the publication No.55 of NUIST Earth System Modelling Center.

References

Blockeel H, Struyf J (2003) Efficient algorithms for decision tree cross-validation. J Mach Learn Res 3:621–650

DelSole T, Shukla J (2009) Artificial skill due to predictor screening. J Clim 22:331–345

Gadgil S, Gadgil S (2006) The Indian monsoon, GDP and agriculture. Economic Political Weekly, Mumbai

Gadgil S, Sajani S (1998) Monsoon precipitation in the AMIP runs. Clim Dyn 14:659–689

Gadgil S, Srinivasan J (2011) Seasonal prediction of the Indian monsoon. Curr Sci 100:343–353

Gadgil S et al (2004) Extremes of the Indian summer monsoon rainfall, ENSO and equatorial Indian Ocean oscillation. Geophys Res Lett 31:L12213

Gadgil S, Rajeevan M, Nanjundiah R (2005) Monsoon prediction—Why yet another failure? Curr Sci 88:1389–1400

Geisser S (1975) The predictive sample reuse method with applications. J Am Stat Assoc 70:320–328

Gill AE (1980) Some simple solutions for heat-induced tropical circulation. Q J Roy Meteor Soc 106:447–462

Gowariker V et al (1991) A power regression model for long range forecast of southwest monsoon rainfall over India. Mausam 42:125

Guhathakurta P, Rajeevan M, Thapliyal V (1999) Long range forecasting Indian summer monsoon rainfallby a hybrid principal component neural network model. Meteorol Atmos Phys 71:255–266

Kalnay E et al (1996) The NCEP/NCAR 40-year reanalysis project. B Am Meteorol Soc 77:437–471

Kang IS et al (2002) Intercomparison of the climatological variations of Asian summer monsoon precipitation simulated by 10 GCMs. Clim Dyn 19:383–395

Kumar KK, Soman MK, Kumar KR (1995) Seasonal forecasting of Indian summer monsoon rainfall: a review. Weather 50:449–467

Kumar KK et al (2006) Unraveling the mystery of Indian monsoon failure during El Niño. Science 314:115–119

Lee J-Y et al (2011) How predictable is the northern hemisphere summer upper-tropospheric circulation? Clim Dyn 37:1189–1203

Lee J-Y et al (2013) Seasonal prediction and predictability of the Asian winter temperature variability. Clim Dyn 41:573–587

Mishra V et al (2012) A prominent pattern of year-to-year variability in Indian Summer Monsoon Rainfall. Proc Natl Acad Sci 109:7213–7217

North GR et al (1982) Sampling errors in the estimation of empirical orthogonal functions. Mon Weather Rev 110:699–706

Rajeevan M (2001) Prediction of Indian summer monsoon: status, problems and prospects. Curr Sci 81:101–107

Rajeevan M et al (2006) High resolution daily gridded rainfall data for the Indian region: analysis of break and active monsoon spells. Curr Sci 91:296–306

Rajeevan M et al (2007) New statistical models for long-range forecasting of southwest monsoon rainfall over India. Clim Dyn 28:813–828

Rajeevan M, Bhate J, Jaswal AK (2008) Analysis of variability and trends of extreme rainfall events over India using 104 years of gridded daily rainfall data. Geophys Res Lett 35:L18707

Rajeevan M, Unnikrishnan CK, Pai DS (2012) Long range forecasting of the Indian summer monsoon. Indian Institute of Tropical Meteorology, Pune

Shukla J, Mooley DA (1987) Empirical prediction of the summer monsoon rainfall over India. Mon Weather Rev 115:695–704

Sinha P et al (2013) Seasonal prediction of the Indian summer monsoon rainfall using canonical correlation analysis of the NCM-RWF global model products. Int J Climatol 33:1601–1614

Sinha P et al (2014) Role of the himalayan orography in simulation of the Indian summer monsoon using RegCM3. Pure Appl Geophys 171:1385–1407

Smith TM et al (2008) Improvements to NOAA's historical merged land-ocean surface temperature analysis (1880–2006). J Clim 21:2283–2296

Smith TM et al (2010) Merged statistical analyses of historical monthly precipitation anomalies beginning 1900. J Clim 23:5755–5770

Wang B, Wu R, Li T (2003) Atmosphere-warm ocean interaction and its impacts on Asian–Australian monsoon variation. J Clim 16:1195–1211

Wang B et al (2005) Fundamental challenge in simulation and prediction of summer monsoon rainfall. Geophys Res Lett 32:L15711

Wang B et al (2007) Coupled predictability of seasonal tropical precipitation. CLIVAR Exch 12:17–18

Wang B et al (2013) Northern Hemisphere summer monsoon intensified by mega-El Niño/southern oscillation and Atlantic multidecadal oscillation. Proc Natl Acad Sci 110:5347–5352

Wang B, Lee JY, Xiang B (2015a) Asian summer monsoon rainfall predictability: a predictable mode analysis. Clim Dyn 44:61–74

Wang B et al (2015b) Rethinking Indian monsoon rainfall prediction in the context of the recent global warming. Nat Commun 6. doi:10.1038/ncomms8154

Webster PJ, Hoyos CD (2010) Beyond the spring barrier? Nat Geosci 3:152–153

Weisheimer A et al (2009) ENSEMBLES: a new multi-model ensemble for seasonal-to-annual predictions: skill and progress beyond DEMETER in forecasting tropical Pacific SSTs. Geophys Res Lett 36:L21711

Xing W, Wang B, Yim S-Y (2014) Peak-summer East Asian rainfall predictability and prediction part I: Southeast Asia. Clim Dyn. doi:10.1007/s00382-014-2385-0